A study of a steering system algorithm for pleasure boats based on stability analysis of a human-machine system model

Fujio Ikeda[1], **Shigehiro Toyama**[1], **Souta Ishiduki**[2] **and Hiroaki Seta**[3]

[1] National Institute of Technology, Nagaoka College, Niigata, Japan
[2] Utsunomiya University, Tochigi, Japan
[3] National Institute of Technology, Toba College, Mie, Japan

E-mail: ikeda@nagaoka-ct.ac.jp

Abstract. Maritime accidents of small ships continue to increase in number. One of the major factors is poor manoeuvrability of the Manual Hydraulic Steering Mechanism (MHSM) in common use. The manoeuvrability can be improved by using the Electronic Control Steering Mechanism (ECSM). This paper conducts stability analyses of a pleasure boat controlled by human models in view of path following on a target course, in order to establish design guidelines for the ECSM. First, to analyse the stability region, the research derives the linear approximated model in a planar global coordinate system. Then, several human models are assumed to develop closed-loop human-machine controlled systems. These human models include basic proportional, derivative, integral and time-delay actions. The stability analysis simulations for those human-machine systems are carried out. The results show that the stability region tends to spread as a ship's velocity increases in the case of the basic proportional human model. The derivative action and time-delay action of human models are effective in spreading the stability region in their respective ranges of frontal gazing points.

1. Introduction

The number of sea disasters relating to maritime accidents of small ships such as pleasure boats has increased in recent years in Japan [1]. The major factors of this trend are increase in the number of beginner captains and complicated manoeuvrability of the pleasure boats. The manual hydraulic steering mechanism (MHSM), which is widely used in these pleasure boats, is known to have poor operability [2]. There are two reasons: the reaction torque of the steering wheel is poor and the steering action tends to lag since the wheel's whole rotation number is a comparatively large 4-7 turns. We have already shown that the poor operability of the MHSM leads to mistakes by beginner captains [3]. One way to improve the poor operability of the steering system is to apply an electronic control steering mechanism (ECSM) by using steer-by-wire (SBW) technology. The SBW has been developed in the area of airplanes and automobiles [4,5]. The SBW enables an operator to generate any reaction torque of the steering wheel and to adjust the rotation angle rate of the steering wheel from the rudder angle in order to improve the operability. However, there are as yet no design guidelines of the control algorithm on how to generate the reaction torque and to decide the rotation angle rate of the steering wheel in the ECSM. Therefore, our study group has started to establish criteria for the design guidelines on the ECSM for pleasure boats.

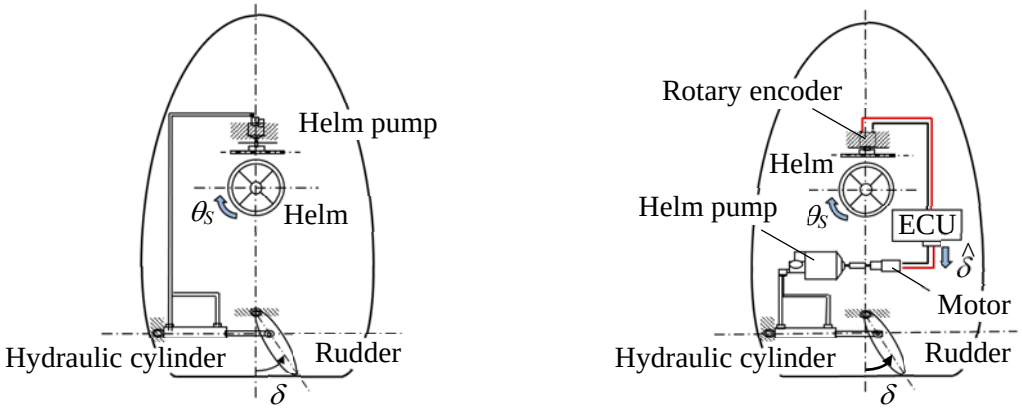

(a) Manual Hydraulic Steering Mechanism (MHSM).

(b) Electronic Control Steering Mechanism (ECSM).

Figure 1. Steering mechanism of pleasure boats.

To aid in establishing the criteria, this paper studies stability analyses of a pleasure boat controlled by human models in view of path following while manoeuvring the ship through a target course. First, we derive the controlled model of the ship in a global coordinate system. Second, we assume several human models to steer and build a closed-loop human-machine controlled system. Third, analytical simulations are carried out to evaluate the stability of those human-machine systems. Last, we show design guidelines of the control algorithm based on the simulation result.

2. Overview of the steering mechanism

2.1. Manual hydraulic steering mechanism

Figure 1(a) shows the manual hydraulic steering mechanism (MHSM), which is the current steering mechanism in common use on pleasure boats. When a captain rotates angle θ_S of a steering wheel (called a helm angle), hydraulic fluid is discharged to the hydraulic cylinder through a helm pump which is directly connected to the steering wheel. Then, a rudder angle δ changes according to movement of a piston rod. Normal pressure N_R is generated on the rudder depending on the rudder angle δ. The moment of rotation at the rudder from the centre of gravity of the hull makes a ship rotate.

The operability of the MHSM is known to be poor because of the following two weaknesses. One is that the captain may have difficulty finding the centre position of the steering wheel when rotating it back after a turn. This is because the full rotation number of the steering wheel from one side to the other side is set on comparatively large values around 4-7, and the reaction torque on the steering wheel is almost isolated. Another reason is that the captain has to master the relationship of the steering wheel movements to the rotational motion of the hull. However, the rotational motion is affected by the normal pressure expressed by equation (5) in Section 3.2, which has complicated nonlinearity in terms of ship's speed V and effective flow angle α. Beginner captains can hardly grasp these dynamics.

2.2. Electronic control steering mechanism

The Electronic control steering mechanism (ECSM), which operates by using steer-by-wire (SBW) technology and is shown in figure 1(b), is considered to be a candidate to improve the poor operability of the MHSM. When a captain rotates angle θ_S of a steering wheel, the angle θ_S is detected by a rotary encoder and input to the electronic control unit (ECU). The ECU outputs a referenced rudder angle signal $\hat{\delta}$ to control a motor, which drives the helm pump, and the following mechanism is the same as the MHSM. By controlling the ECU, the ECSM can translate precisely the steering angle to the rudder angle without excess rotations of the steering wheel. In addition, the reaction torque on the steering

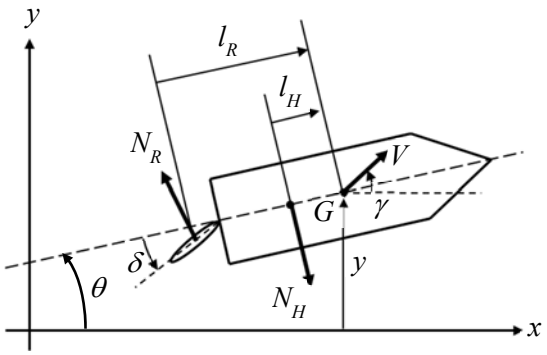

Figure 2. Motion model of pleasure boats in global coordinate system.

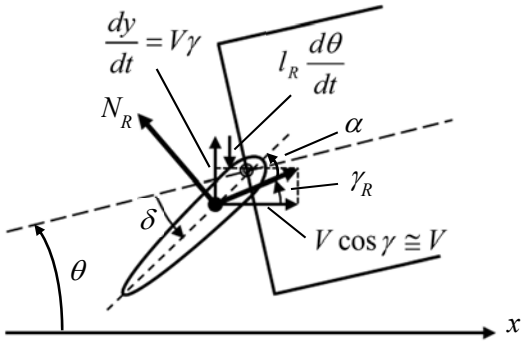

Figure 3. Schematic of acting forces around the rudder.

Table 1. Parameters for motion model of pleasure boat.

Parameter	Description	Parameter	Description
G	Centre of gravity	N_R	Normal pressure
m	Mass	N_H	Turning resistance
I	Moment of inertia	l_R	Distance between centre of gravity and action point of normal pressure
y	Lateral displacement		
θ	Heading angle	l_H	Distance between centre of gravity and action point of turning resistance
δ	Rudder angle		
γ	Angle of boat speed from x axis	γ	Angle of boat speed from x axis
		T	Propulsive force of propeller
		D	Fluid resistance force of hull

wheel can be generated. If any algorithms to appropriately control these complicated behaviours would be developed, then operability of the steering system would be expected to improve. However, the control algorithm of the ECSM has not yet been clarified.

3. Dynamics of a pleasure boat model

To analyse stability in view of path following of the target course by the pleasure boat controlled by human models, we consider the human-machine system which integrates models of pleasure boats and humans. This section derives equations of motion of pleasure boats.

3.1. Equations of motion of pleasure boats in the global coordinate system

Conventional ship motions in the horizontal plane are written in the body-referenced coordinate affixed on the body where the origin is the centre of gravity. However, for the above objective, ship motions have to be written in the global-referenced coordinate affixed on the sea, as shown in figure 2. The motion frame has forward direction x-axis, sway to the left direction y-axis and yaw rotation. The parameters for the motion model are listed in table 1. The equations of motion are represented by a surge, a sway and an angular motion as follows:

$$m\frac{d^2x}{dt^2} = T\cos\gamma - D, \tag{1}$$

$$m\frac{d^2y}{dt^2} = N_R\cos(\delta+\theta) - N_H\cos\theta, \tag{2}$$

$$I\frac{d^2\theta}{dt^2} = -l_R N_R\cos\delta + l_H N_H. \tag{3}$$

We assume the forward directional velocity of the boat has constant speed V, therefore the motion of forward direction (1) is uncoupled. This paper only deal with the equations of motion (2) and (3) to examine the stability analysis.

3.2. Linear approximation of equations of motions

To examine the stability analysis of the ship motion, equations (2) and (3) are approximated to obtain linear input-output relations from the rudder angle δ to the lateral displacement y and heading angle θ. We consider the boat is navigated almost along a straight line, because the boat is always controlled by a human. Therefore, the heading angle and rudder angle are assumed to be small enough and become $\cos\theta \cong 1$ and $\cos(\theta+\delta) \cong 1$. Then, equations (2) and (3) are written as follows:

$$m\frac{d^2y}{dt^2} = N_R - N_H, \tag{4}$$

$$I\frac{d^2\theta}{dt^2} = -l_R N_R + l_H N_H. \tag{5}$$

The normal pressure N_R and turning resistance N_H should be derived in a concrete form, respectively. First, the normal pressure N_R is expressed by the following formula [6]:

$$N_R = f_R V^2 \sin\alpha \tag{6}$$

where f_R is coefficient of normal pressure, derived in Section A of the Appendix, V is ship's speed, and α is effective flow angle expressed as follows:

$$\alpha = \delta + \theta - \gamma_R, \tag{7}$$

where γ_R is an angle formed by moving direction at the rudder position and x-axis, which is called slip angle of the rudder shown in figure 3. We suppose the slip angle at the centre of gravity of the hull is small enough $|\gamma| << 1$, the hull moves at the translational motion of the component toward x-axis $V\cos\gamma \cong V$ and the component toward y-axis $V\sin\gamma \cong V\gamma = dy/dt$, together with the rotational motion around the centre of gravity $d\theta/dt$. These forces are balanced at the rudder. Hence, the slip angle of the rudder is

$$\gamma_R \cong \tan\gamma_R = \frac{V\gamma - l_R \cdot d\theta/dt}{V} = \frac{1}{V}\frac{dy}{dt} - \frac{l_R}{V}\frac{d\theta}{dt}. \tag{8}$$

Consequently, by assuming $|\alpha| << 1$, the normal pressure written as equation (6) is described by

$$N_R \cong f_R V^2\left(\delta + \theta - \frac{1}{V}\frac{dy}{dt} + \frac{l_R}{V}\frac{d\theta}{dt}\right). \tag{9}$$

Next, the turning resistance N_H is proportional to the heading angular velocity

$$N_H = c\frac{d\theta}{dt}, \tag{10}$$

where c is coefficient of normal pressure, described in Section B of the Appendix. Substituting equations (9) and (10) into equations (4) and (5), the equations of motion of pleasure boats in the global coordinate system are described as

$$m\frac{d^2y}{dt^2} + f_R V\frac{dy}{dt} + \left(c - l_R f_R V\right)\frac{d\theta}{dt} - f_R V^2\theta = f_R V^2\delta, \tag{11}$$

$$I\frac{d^2\theta}{dt^2} - l_R f_R V\frac{dy}{dt} - \left(cl_H - l_R{}^2 f_R V\right)\frac{d\theta}{dt} + l_R f_R V^2\theta = -l_R f_R V^2\delta. \tag{12}$$

Taking the Laplace transform of equations (11) and (12), the transfer functions from the input δ to the outputs y and θ can be represented as follows.

$$G_y(s) = \frac{If_R V^2 s + \left(l_R - l_H\right)f_R V^2 c}{mIs^3 + \left\{If_R V + m\left(l_R{}^2 f_R V - l_H c\right)\right\}s^2 + \left\{ml_R f_R V^2 + \left(l_R - l_H\right)f_R Vc\right\}s} \tag{13}$$

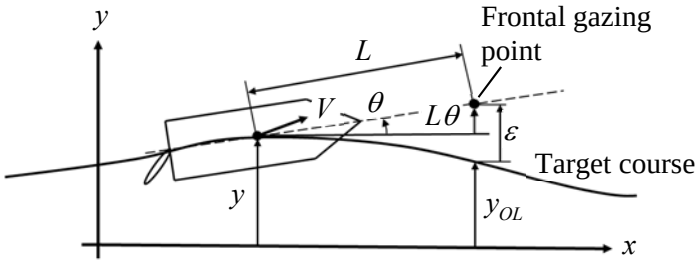

Figure 4. Motion of pleasure boats to follow the target course.

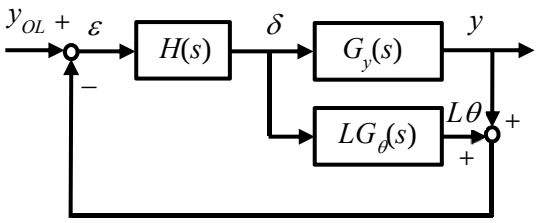

Figure 5. Brock diagram of closed-loop human-machine system model.

$$G_\theta(s)=\frac{-ml_R f_R V^2 s}{mIs^3+\{If_R V+m(l_R{}^2 f_R V-l_H c)\}s^2+\{ml_R f_R V^2+(l_R-l_H)f_R Vc\}s} \tag{14}$$

4. Stability analysis of the pleasure boat controlled by human models

In this section, we design and make the human-machine feedback systems consisting of several human models and the previously mentioned pleasure boat model.

4.1. Human-machine system model

We set the pleasure boat a task to follow the target course in almost a straight line, as shown in figure 4. L is distance between centre of gravity and a frontal gazing point, and y_{OL} is lateral displacement of the target course at a looking ahead point. Therefore, the error between the actual course and the target course is derived as follows:

$$\varepsilon = y_{OL} - (y + L\theta) \tag{15}$$

Figure 5 shows the block diagram of the path following the feedback system including human model from input of the target course to the output of the actual course. The block of $H(s)$ is the control model of the human dynamics described in the next section.

4.2. Control model of the human dynamics

A number of studies concerned with the control model of the human dynamics have been presented [7]. One approach is to describe human dynamics as transfer function models $H(s)$ which regard human behaviour as linear continuous feedback models. We employ this approach and describe the human dynamics as a classical proportional-integral-derivative (PID) plus time-delay transfer function, which is given by

$$H(s) = h\cdot\left(\tau_D s + 1 + \frac{1}{\tau_I s}\right)\cdot \mathrm{e}^{-\tau_L s}. \tag{16}$$

We human beings can naturally steer proportional to the error signal, and h is the proportional gain constant. We can also forecast the movement in a short time to come; this is the operation of the derivative which has a coefficient of τ_D. On the other hand, we can move the shifted position back to the centre position; this is the operation of the integral which has a coefficient of τ_I. We experience a time delay of a few seconds in the steering; τ_L is the time delay constant. The transfer function of equation (16) is the combination of the above four features.

4.3. Closed-loop system in view of path following

The transfer function of the closed-loop system in view of path following of the target course (i.e., the transfer function from y_{OL} to y in figure 5 is obtained as

$$G(s)=\frac{b_1 sH(s)+b_0 H(s)}{a_3 s^3+a_2 s^2+(a_{11}+a_{12}H(s))s+a_0 H(s)} \tag{17}$$

where the coefficients are described as follows:

$$a_3 = mI,\ a_2 = If_R V + m\left(l_R{}^2 f_R V - l_H c\right),\ a_{11} = ml_R f_R V^2 + \left(l_R - l_H\right) f_R V c,\ a_{12} = \left(I - Lml_R\right) f_R V^2,$$
$$a_0 = \left(l_R - l_H\right) f_R V^2 c,\ b_1 = If_R V^2,\ b_0 = L\left(l_R - l_H\right) f_R V^2 c.$$

In the next section, we derive a characteristic equation which is the denominator of equation (17) for each human model. As varying parameters of manoeuvring condition V, L and the human model h, τ_D, τ_I, τ_L, we determine the stability regions from these characteristic equations whose roots are all negative.

5. Stability analysis by simulation

5.1. Conditions of analysis

The pleasure boat is supposed to be a standard small vessel whose parameters are listed in Section B of the Appendix [8]. The ship's speed V, the distance between centre of gravity and a frontal gazing point L, and the proportional gain h are variable design parameters. V is varied from 6.8 m/s (=13.3 kt) to 8.8 m/s (=17.1 kt), which are within a usual operation range, according to the change of propeller revolution N described in Section A of the Appendix. L is from 1 to 500 m, and h is varied from 0.001 to 1 rad/m; both of these parameters are referred to in [7].

5.2. Proportional action of human model

First, to check the fundamental property of the human model, we suppose that all human model parameters except proportional gain h are zero; the transfer function $H(s)$ of equation (16) is described by

$$H(s) = h\,. \tag{18}$$

Then, the characteristic equation is given by

$$a_3 s^3 + a_2 s^2 + \left(a_{11} + a_{12} h\right) s + a_0 h = 0\,. \tag{19}$$

If all of the roots of equation (19) are negative, then the system is stable. Figure 6 shows the upper bound of stability region for each value of V in the L-h plane. These lines indicate that the ship's velocity is higher and the stability region is wider. It should be noted that the rate of increase of the stability region is nonlinear with regard to the increase of the ship's velocity. Furthermore, the stability region passes away at the lowest speed V = 6.8 m/s. In addition to these, this figure indicates that the gain h slightly falls as L becomes longer.

5.3. Adding derivative action with proportional action of human model

Second, we suppose the transfer function $H(s)$ of human dynamics has proportional and derivative action as follows:

$$H(s) = h\left(\tau_D s + 1\right), \tag{20}$$

where the coefficient of derivative is set to τ_D = 0.2 s. Then, the characteristic equation is given by

$$a_3 s^3 + \left(a_2 + a_{12} h \tau_D\right) s^2 + \left(a_{11} + a_{12} h + a_0 \tau_D\right) s + a_0 h = 0\,. \tag{21}$$

Figure 7 shows the upper bound of the stability region for each value of V in the L-h plane. Compared to the only proportional action of equation (18), adding derivative action, which means forecasting the future movement, this leads to spreading the upper bound of the stability region. On the other hand, as the frontal gazing point L is over 100 meters long, the stability regions sharply drop. The main reason is that the error of lateral displacement between the actual course and the target course is regarded as a relatively large value in the case of the long distance of L. Accordingly, the large error causes excessive input of the rudder angle, so that gain h should be smaller to follow stably.

5.4. Adding integral action with proportional action of human model

Third, we suppose the transfer function $H(s)$ of human dynamics has proportional and integral action as follows:

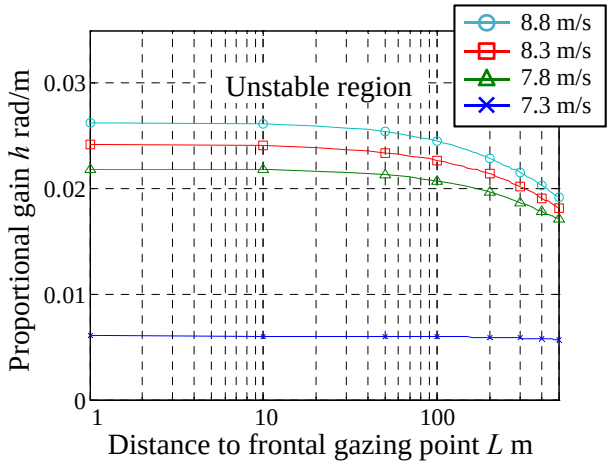

Figure 6. Stability region in *L*-*h* plane in the case of $H(s) = h$.

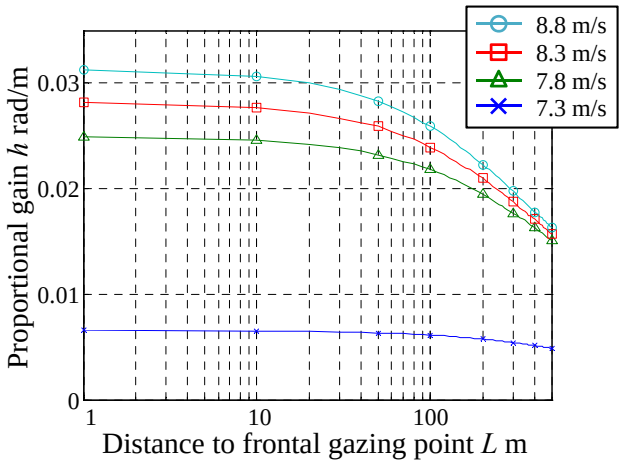

Figure 7. Stability region in *L*-*h* plane in the case of $H(s) = h(\tau_D s + 1)$.

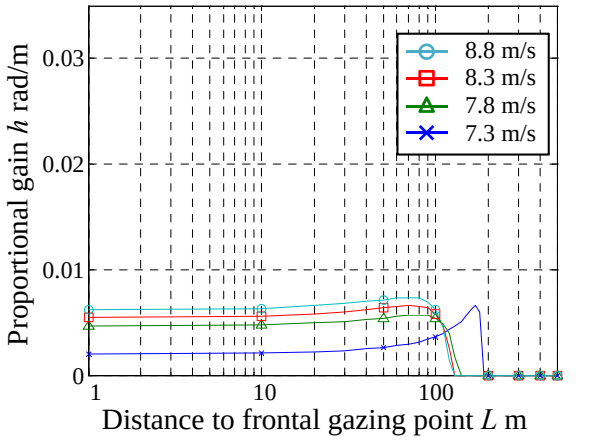

Figure 8. Stability region in *L*-*h* plane in the case of $H(s) = h(1 + 1/\tau_I s)$.

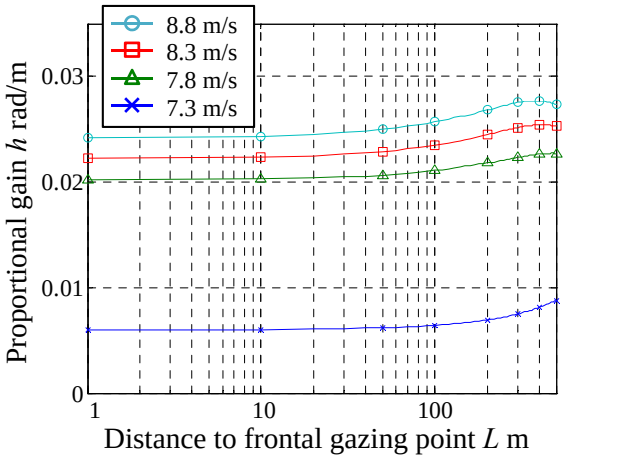

Figure 9. Stability region in *L*-*h* plane in the case of $H(s) = he^{-\tau_L s}$.

$$H(s) = h\left(1 + \frac{1}{\tau_I s}\right), \tag{22}$$

where the coefficient of integral is set to τ_I = 0.2 s. Then, the characteristic equation is given by

$$a_3\tau_I s^4 + a_2\tau_I s^3 + (a_{11} + a_{12}h)\tau_I s^2 + (a_{12} + a_0\tau_I)hs + a_0 h = 0\,. \tag{23}$$

Figure 8 shows the upper bound of the stability region for each value of *V* in the *L*-*h* plane. Compared to the only proportional action of equation (18), adding integral action, which has the effect of eliminating offset, leads to a drastically reduced upper bound of the stability region. Moreover, the stability region for every ship's speed vanishes when *L* is over 100 meters. That is because the integral action has a phase component of -90degrees, and the additional phase lag of 90degrees reduces the phase margin of the system.

5.5. Adding time-delay action with proportional action of human model

Finally, we suppose the transfer function *H*(*s*) of human dynamics has proportional and time-delay action as follows:

$$H(s) = he^{-\tau_L s} \cong \frac{h\left(1 - \frac{\tau_L}{2}s\right)}{1 + \frac{\tau_L}{2}s} \tag{24}$$

$$\cong \frac{h}{1+\tau_L s} \tag{25}$$

where the coefficient is set to τ_L = 0.35 s. The last term of equation (24) is Pade approximation, and equation (25) is approximated by a first-order delay for the time delay, respectively. In the case of Pade approximation model of equation (24), the characteristic equation is given by

$$a_3 \tfrac{\tau_L}{2} s^4 + \left(a_3 + a_2 \tfrac{\tau_L}{2}\right)s^3 + \left(a_2 + \tfrac{\tau_L}{2}\left(a_{11} - a_{12}h\right)\right)s^2 + \left(a_{11} + h\left(a_{12} - a_0 \tfrac{\tau_L}{2}\right)\right)s + a_0 h = 0\,. \tag{26}$$

While in the case of a first-order delay model of equation (24), the characteristic equation is given by

$$a_3\tau_L s^4 + \left(a_3 + a_2\tau_L\right)s^3 + \left(a_2 + a_{11}\tau_L\right)s^2 + \left(a_{11} + a_{12}h\right)s + a_0 h = 0\,. \tag{27}$$

The property of stability region of these two approximation models is almost the same, though the first-order delay model in equation (25) is somewhat outperformed for the effectiveness to extend the stability region. Therefore, we show the stability region of the first-order delay model for each value of V in the L-h plane in figure 9. Compared to the only proportional action of equation (18), adding time-delay action makes the upper bound of h slightly lower for the short range of L. On the other hand, the upper bound of h is raised around the long range of L. That is because the time-delay model plays a role of a low-pass filter to cut off too much input of the rudder angle.

5.6. Discussion for design guidelines of control algorithm in ECSM

Based on the previously obtained simulation results, we discuss the design guidelines in order to spread the stability regions of the human-machine system. We found that the stability region can be spread by adding or emphasizing the derivative action, when distance to the frontal gazing point L becomes relatively close (such as in coastal areas or around obstacles). On the other hand, when distance to the frontal gazing point L becomes relatively far (such as offshore situations or around few obstacles), the stability region can be spread by adding or emphasizing the time-delay actions.

If a beginner captain navigates around an onshore area whose location is estimated by using an inertial navigation system (INS) or global positioning system (GPS), then a frontal gazing point L should be assumed to be short. In such a situation, the ECSM shown in figure 1(b) can add the derivative model, which spreads the stability region, to the standard human model in order to improve the operating performance. Likewise, if a beginner captain navigates around an offshore area, then L should be assumed to be relatively long. In such a situation, the ECSM can add the first-order delay model, which recovers the stability region, to the standard human model in order to prevent deterioration in the operating performance. It should be noted that the above results are obtained under assumption on a linear approximation of small rudder angle, and maneuvering situation with large rudder angle is out of consideration.

6. Conclusions

This paper studies stability analyses of a pleasure boat controlled by human models in view of path following of the target course, in order to help establish the criteria for the design guidelines of the ECSM. First, the controlled model of the boat is made by linear approximation and its transfer function is derived. Then, several human models to steer are assumed and closed-loop human-machine controlled systems are developed. The stability analysis simulations for those human-machine systems are carried out and the following results are obtained:

- The higher the ship's velocity is, the higher the upper bound of the stability region is for the case of the standard human model of proportional motion.
- The human model with derivative action added can spread the stability region in the situation of the short range of the frontal gazing point.
- The human model with time-delay action added can spread the stability region in the situation of the long range of the frontal gazing point.

Further studies can be conducted on the use of the ECSM on pleasure boats. For example, manoeuvrability testing by ship simulator will verify the effects of installing derivative action and time-delay action models. Some of the human parameters which differ from person to person will also

be identified. Moreover, maneuvering situation over the linear range of small heading and rudder angle need to be examined.

Acknowledgements
This study was partially supported by a Grant-in-Aid for Scientific Research (C) No. 25350487 from the Japan Society for the Promotion of Science (JSPS), for which the authors express their deepest gratitude.

Appendix

A. Coefficient of normal pressure

The coefficient of normal pressure f_R written in equation (6) is known to be described as follows [6]:

$$f_R = \frac{\rho}{2} A (1-w)^2 (1+3.6S^{1.5}) \frac{6.13\lambda}{\lambda+2.25} \tag{A.1}$$

where ρ is water density, A is rudder area, w is wake coefficient, λ is aspect ratio of rudder, and S is real slip ratio described by

$$S = 1 - \frac{V}{P \cdot N} \tag{A.2}$$

where P is propeller pitch and N is propeller revolution. N is related to the ship's speed V, and the relationship between N and V in steady state, when the boat is traveling on a straight line, is shown in figure A.1. This figure indicates that the relation between N and V is almost linear.

B. Parameters of pleasure boat

The pleasure boat for the stability analysis is supposed to be a standard small vessel whose constant values of the parameters in the transfer function of equation (17) are listed in table B.1 [8]. The moment of inertia I and the coefficient of normal pressure c are varying parameters according to V and are described as follows:

$$I = \frac{T}{K} l_R f_R V^2, \tag{B.1}$$

$$c = \frac{l_R f_R}{K l_H} V^2. \tag{B.2}$$

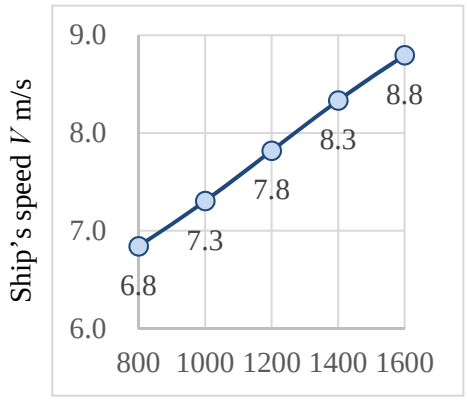

Figure A.1. Relationship between propeller revolution N and ship's speed V.

Table B.1. Parameters for stability analysis of pleasure boat.

Parameter	Value	Unit	Description
l	12.5	m	Length of boat
m	1.31×10^4	kg	Mass of boat
l_R	4.50	m	Distance between centre of gravity and action point of normal pressure
l_H	0.392	m	Distance between centre of gravity and action point of turning resistance
ρ	1.00×10^3	kg/m^3	Water density
A	0.260	m^2	Rudder area
w	0.225	–	Coefficient of wake
λ	1.90	–	Aspect ratio of rudder
P	0.810	m	Propeller pitch
T	3.46	s	Index of responsiveness to the helm
K	0.888	1/s	Index of turning ability

References

[1] Cabinet Office of Japan 2015 Maritime Accident Trends *White Paper on Traffic Safety in Japan* pp 109-114
[2] Ikeda F, Toyama S, Seta H and Ezaki N 2011 Improvement of Steering Feeling on Maneuverability for Pleasure Boat *Journal of System Design and Dynamics* **5** 5 pp 1119-1126
[3] Iihama K, Toyama S, Ikeda F, Seta H and Ezaki N 2013 Operability Evaluation of Pleasure Boats Based on Usability as Addressed by ISO 9241-11 Trans. of the JSME, Ser. C **79** 801 pp 1415-1426
[4] Tanaka Y and Kobayashi M 1998 Evolution of Aircraft Flight Control Actuation System *The Journal of IEICE* **81** 9 pp 932-938
[5] HONDA 2016 Chassis VGS *Chassis Technology* http://www.honda.co.jp/tech/auto/chassis/vgs/ (accessed on 10 Feb 2016)
[6] Okada S 1964 Feature and Design of Rudder *The Society of Naval Architects of Japan* **424** pp 809-823
[7] Abe M 2008 Automotive Vehicle Dynamics (Tokyo Denki University Press) chapter 9 pp 223-243
[8] Inoue K 2011 Theory and Practice of Ship Handling (Seizando) chapter 2 pp 25-68